2024 IEEE International Conference on Robotics and Automation (ICRA 2024)
May 13-17, 2024. Yokohama, Japan

Mechanism Design for New Sensors Field Deployment by LineRanger Powerline Robot

Pierre-Luc Richard, Jonathan Bellemare, Philippe Hamelin, Camille Hébert, Ghislain Lambert, Samuel Lavoie, Sébastien Leprohon, Matthieu Montfrond, Marion Nourry, Alex Sartor, Nicolas Pouliot

Abstract— **Powerline robotics is slowly becoming key tools for electric utilities. Contrary to drones that are usually limited to inspection tasks, wheeled robots like LineRanger can perform a broader range of applications. In this paper, a suite of mechanical devices is featured, as several new asset management tasks were recently added to LineRanger's capabilities. While previous applications focused on non-contact inspection (visual, electro-magnetic, etc.), the new tasks at hand involved *reaching* adjacent conductors to probe line components with micro-Ohmmeter, *installing and retrieving* custom build sensors for multi-day line monitoring, and *assessing* aging conductors surface properties, to refine their thermal model and optimize the line capacity during heat waves. All three applications were recently field validated onto LineRanger, and mechanical design insights shall be presented for each module.**

Keywords: Field robotics, mechanism design, transmission line inspection

I. Introduction

Figure 1. LineRanger rolling on live large river crossing spans.

Power lines are, and will remain, instrumental assets to support the energetic transitions towards a decarbonized economy. To play that role, they must be erected, operated, inspected and maintained in an optimal manner. Almost 20 years ago, this is why Hydro-Quebec undertook a comprehensive power line robotic program that has supplied a suite of mobile platforms, including LineDrone [1][2], and advanced sensors [3]-[6]. These and other initiatives [7]-[13] are slowly but surely opening the way for a possible revolution where advanced robotic systems can add up to the different asset management options available.

Among the different robots, LineRanger [14]-[16] is becoming a solution of choice for evolving on double or quad bundles conductors. Since last published work [17], LineRanger was used on a few dozens of occasions, had reached its 4th design evolution, gained the possibility of being troubleshooted over LTE mobile network and is now part of a training program within Hydro-Quebec to formally incorporate LineDrone and LineRanger usage into regular operations.

As a reminder, part of LineRanger internal success relies on its applied design philosophy: being light, fast moving (8 km/h), quick at surpassing obstacles (< 5 sec) and much simple to operate but without any compromise on versatility/modular approach as emerging needs arise. The initial design strategy of minimizing weight, limiting number of motors and internal cabling, counting on mechanical subsystems paid off: relying on optimized mechanical devices and clever systems allows to easily deploy newly developed sensors, while ensuring intrinsic reliability despite such a harsh environment. The contributions of the paper are three (3) new robotic applications of LineRanger on live lines through the deployment of new sensors. These deployments are possible thanks to new assisting passive mechanical devices for which design details are provided. All that broaden the scope of this valuable mobile robot.

II. Compact and Strong 2-DoF Deployable Arm

Splices are used to connect sections of conductors, allowing for line changes of direction, or to perform repairs. There are therefore tens of thousands of these line components, and they must sustain both mechanical and electrical heavy loadings. Defective splices are either due to improper installation or the aging effect of environment pollutant that penetrates inside. Both generate an increase of the electrical resistance, so their condition is ideally assessed by measuring a micro-Volts difference between their junctions, while current flows through the powerline. This is a lot more precise than inspection from a distance with thermal imagery but requires reaching the splice and precisely locate sensor on live conductor. For quad-bundled conductors, and since LineRanger runs on the lower pair of conductors, only these ones used to be accessible by sensors. Then, to reach and measure splices on the above conductors, a new compact, lightweight but strong mechanical arm is designed. The system presented in the following section is versatile enough to perform other tasks, avoiding lineman to be suspended from a helicopter or to walk on live lines.

A. *Mechanical design*

To fulfil this task with a robot, many constraints must be considered. The range of motion must be considerable to reach top conductors (~0,5 m), plus adding-up the distance increase due to the robot's weight (~0.2 m). And the force must also be enough to either lift a high payload or to apply high contact force on the conductor (80-100 N).

*All the authors are with of Hydro-Québec's research institute (IREQ) in Varennes, CANADA. (Pierre-Luc Richard can be reached as corresponding author at 1-450-652-8085 or at richard.pierre-luc@hydroquebec.com).

From a design point of view, the mechanism must be light and compact to be deployed on LineRanger without significantly affecting the payload of the robot. Compactness is crucial to avoid interfering with obstacle crossing capabilities. Motors must be limited to the minimum necessary to achieve the task while being as small as possible to reduce its weight. Finally, it is important to keep the tool in a constant orientation for stability.

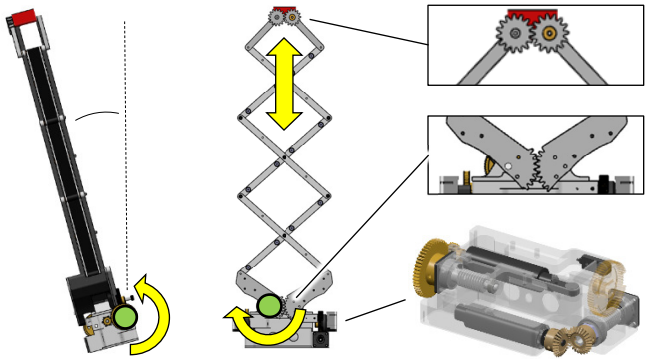

Figure 2. 2-DoF deployable light mechanism for powerline robot.

Different approaches were evaluated before the design: a classical serial robotic arm, a telescopic arm, and a deployable scissor mechanism. Among these three, the best option is a scissor deployable mechanism mounted on a pivot, using it to align the moving plane with the conductor. It combines large reach, lightness, and compactness while large force can be obtained through optimization (shown later).

As seen on Figure 2 (right side), two sets of gears are used to 1/ synchronize the two first links at the bottom and 2/ to have a constant orientation of the effector at the top. Two motors (for rotation and extension) are mounted inside a transmission box at the bottom, so their weight is not considered in the payload. A hybrid assembly, wisely combining aluminum/plastic parts optimizes rigidity versus weight and, finally, electrical continuity is implemented to guarantee proper usage on live lines.

B. Optimization and gravity compensation

An optimization with a mathematical model is crucial to keep the mechanism small and light while developing high force. The main reason is that the higher the number of scissors stages, the lower is the available force at effector because each stage acts as a torque reductor, as shown below.

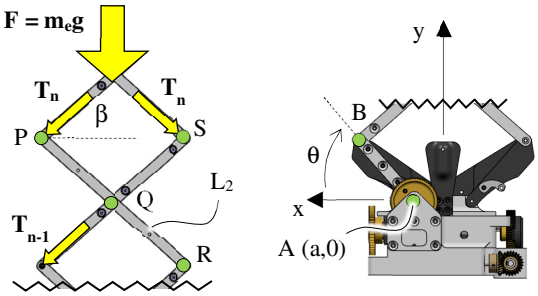

Figure 3. Force analysis of deployable mechanism.

Figure 3 shows that the force in the nth link is found directly while the force in the second link (PR) is given by studying point S and doing the sum of moments at point R (1). Expanding the same calculation through all the n stages and combining both sides of links, the force at the effector seen at the first link, the motorized one, is given by (2).

$$T_n = \frac{F}{2sin\beta} \quad \text{and} \quad T_{n-1} = \frac{F}{2sin\beta} \cdot (2 - cos\beta) \tag{1}$$

$$T_i = \frac{F}{sin\beta} \cdot (2 - cos\beta)^{n-i} \tag{2}$$

Hence, tension in links increases greatly with the number of stages. Similarly, weight of the moving parts (the *n* stages of mass m_s) must be considered and can be found with:

$$W = \sum_{i=1}^{n} W_i = \sum_{i=1}^{n} \frac{m_s g}{sin\beta} \cdot (2 - cos\beta)^{n-i} \tag{3}$$

As links have many revolute joints in which there is friction, this effect on the motor must also be considered. To evaluate the potential gain of using bearings instead of bushings, the torque generated by the friction in joints is approximated by the following equation:

$$M_f \geq \sum_{i=1}^{n} M_{f_i} = \sum_{i=1}^{n} \mu \frac{T_i d}{2} N \tag{4}$$

Where *N* is the number of joints by stage and *d* the diameter of the pin of the joint and μ, the coefficient of friction (0.5 for bushings, ~0 for bearings). Combining all above equations, the torque *M* at the motor is given by:

$$M = \frac{F \cdot (2 - cos\beta)^{n-i}}{sin\beta} q + \sum_{i=1}^{n} \left(\mu \frac{T_i d}{2} N + \frac{m_s g \cdot (2 - cos\beta)^{n-i}}{sin\beta} q \right) \tag{5}$$

Where

$$q = L_1 \frac{sin(\theta+\beta)}{sin\beta}, \ \beta = \text{acos}\left(\frac{B_x}{L_2}\right) \text{ and } B_x = a + L_1 cos\theta$$

These equations are used to optimize the mechanism (Figure 4). Using the minimum number of stages to reach the conductors (here, 3), built with hybrid links made of aluminum and plastic and, replace the intuitive simple solution of bushings by rolling bearings reduce, the torque is reduced by ~40%, reducing the motor size and overall weight.

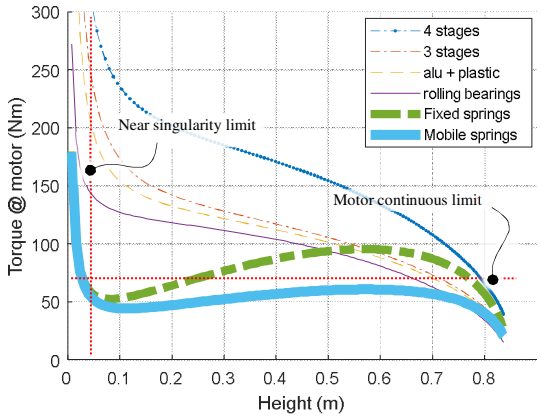

Figure 4. 2-DoF deployable mechanism optimization for 8 kg payload.

However, to further increase its payload, extending its capacities by compensating the gravity is necessary. Due to space and compactness requirements combined with the

reduction stage property, effective gravity compensation is hardly achievable with only one (fixed) spring configuration.

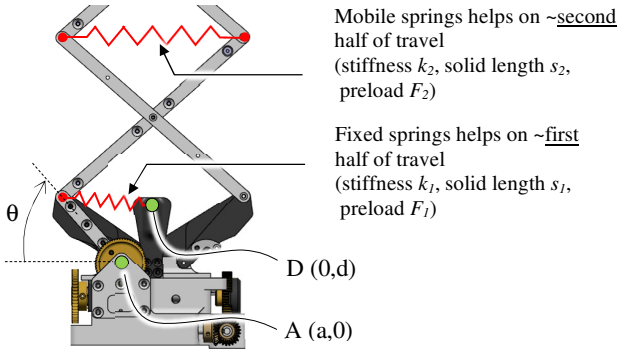

Figure 5. Gravity compensation of 2-DoF deployable mechanism.

A combination of two springs (fixed and mobile) helps the motor during two distinct phases of reach (Figure 5). The torque M_s generated by both springs is then added to (5):

$$M_s = \left(k_1\left(\sqrt{(a + L_1 cos\theta)^2 + (L_1 sin\theta - d)^2} - s_1\right) + F_1\right) \cdot sin\gamma + \left(k_2(L_2 cos\beta - s_2) + F_2\right) \cdot sin\theta \quad (6)$$

Where $\gamma = \tan^{-1}((d - L_1 sin\theta)/B_x)$. L_1, L_2 and points A and D have been chosen to maximize M_s considering interferences and spring availability. Results are shown on bold curves of Figure 4. Torque at 0.05 m travel is reduced by a factor > 5 after optimization and gravity compensation. The mechanism weights 3.1 kg and has a payload of 8 kg on a reach of 0.85 m except under 0.05 m. In this singularity "zone", links would be nearly all aligned ($\theta = \beta \sim 0$). That can be avoided by setting the initial position higher, which is intrinsically part of the design since all the links rely on each other setting then a "minimum thickness" to the retracted state. Springs can be added depending on the force required.

C. Field deployment

A prototype was built and used on live 735 kV powerline for actual splices condition assessment, on all-four conductors, which is a world first among the powerline field robotics community. The pictured LineOhm sensor weights 0.5 kg.

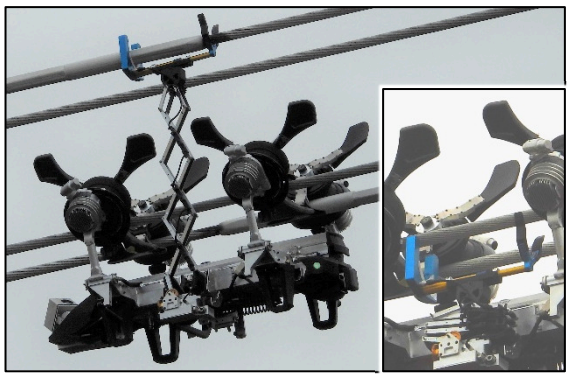

Figure 6. Field deployment for electrical resistance measurement.

III. Dual Action Latching System

Like any metallic components, powerline conductors tend to expand in proportion of their average temperature. Sun radiations and high currents will heat them up, while local wind will cool them down. This temperature change will in-turn be reflected in any span by a sag increase or decrease, therefore varying the minimum distance to the ground. The goal is to very precisely measure a given span and extrapolate its sag during heat waves or maximum line loadings, when conductors can reach 75 °C (or more). For that purpose, a high precision contacting sensor that measures the outside temperature and the GPS location (PPK corrected) was designed, and a series of them must be installed to monitor the line for a window of time (4 h to mechanism described in Section II was instrumental at deploying these sensors, as they needed to be installed on the upper conductor of a bundle, to avoid blocking LineRanger's travelling ability. This sensor, tagged *Chronos*, hold onto the line through spring-loaded clamps so there was the need to devise a clamp/release (dual action) latching mechanism, without adding any electrical device or motor to keep the robot simple, while securely holding on the 2.0 kg sensor.

Common double state systems (ex.: push button) require an additional unlocking movement prior to retracting. For a teleoperated robot, it is better avoiding these delicate operations that could put at risk the locking/unlocking function. The objective is to develop a mechanism that, once the sensor is installed on the conductor, is simultaneously ready to be re-latched, without any other manipulation than an automatic snapping. The following challenging behavior is desired: phase 1/ snap the sensor on the conductor while unlocking the effector, phase 2/ retract the effector while resetting the mechanism, phase 3/ re-insert the effector and locking the effector and, phase 4/ retract the sensor from the conductor. To the knowledge of the authors, such system was not previously designed and is not commercially available.

A. Mechanical design

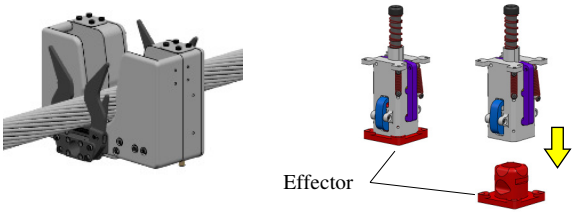

Figure 7. *Chronos* sensor and latching mechanism.

To get a such challenging behavior, the sensor is combined with a clever latching mechanism (Figure 7). Figure 8 and 9 and the accompanying video explain the mechanism that is enabled with a downward movement of the plunger upon contacting the conductor through the sensor (also Figure 10, red circle), thus unlocking the red effector. The plunger pushes on two yellow hooks (1), forcing down the green part that simultaneously pushes on both purple hooks (2) to unlock the red effector (3).

The effector is retracted from the mechanism, resetting it at the same time. With the effector two different cross sections, a wedge of the effector makes the blue part rotate (4). This rotation also makes the two yellow hooks rotate (5) and clear their tips from the plunger (6), opposite to step (1). Springs bring back up the green part upward (7). The yellow hooks tips are now over the plunger (8) and the purple hooks

are brough back at their initial position with springs (9). In this configuration, the red effector can be re-inserted inside the mechanism to be latched again. By releasing the force on the plunger, it comes back over the yellow hooks' tips (10).

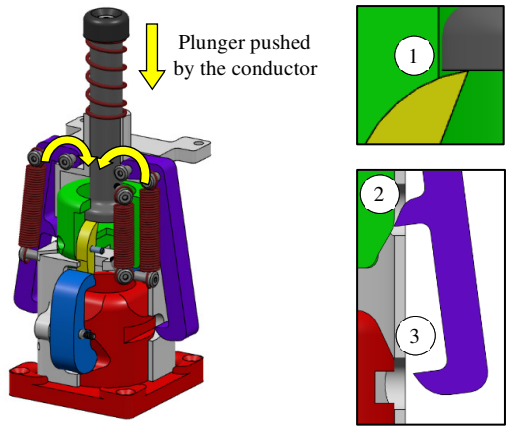

Figure 8. Enabling the mechanism, unlocking the effector.

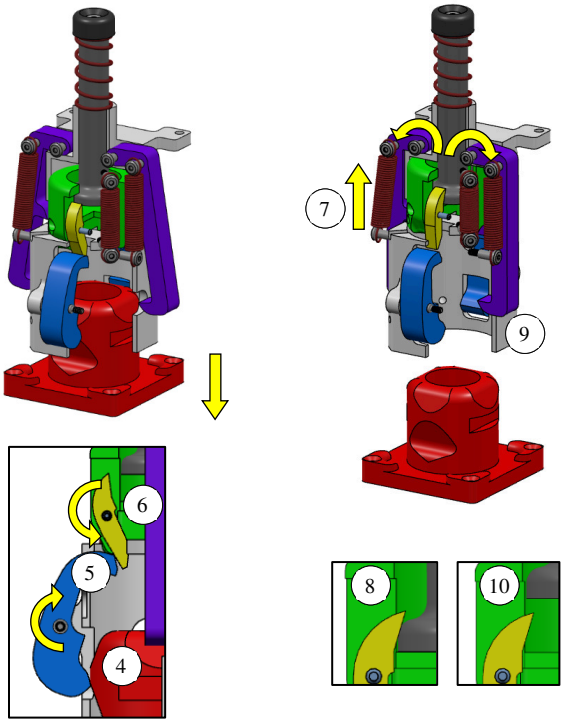

Figure 9. Removing the effector, resetting the mechanism.

B. *Combination with a sensor*

Using the above-described innovative latching mechanism, a sensor can easily be installed and uninstalled on a conductor by simply pushing up and down the effector. The sensor is approached from the conductor (Figure 10). When installed, it pushes on the plunger, circled in red on the figure, unlatching the effector (steps 1 to 3). The effector can then be retracted, resetting the mechanism (steps 4 to 9) and letting the sensor on the conductor, held by its own support hooks. To retrieve it, the effector is simply re-inserted in the mechanism, being automatically locked by the purple hooks. By lowering the mechanism and sensor away from the conductor, the plunger is released, ready to be re-installed.

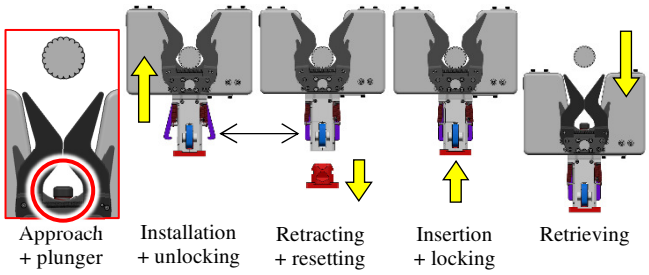

Figure 10. Sensor installation sequence.

C. *Field testing*

The mechanism and the sensor have been integrated on LineRanger and deployed with its new strong deployable mechanism. Thanks to its high force and long reach, the *Chronos* sensor has been easily installed on the top conductors of a bundle. It has been brought back as easily.

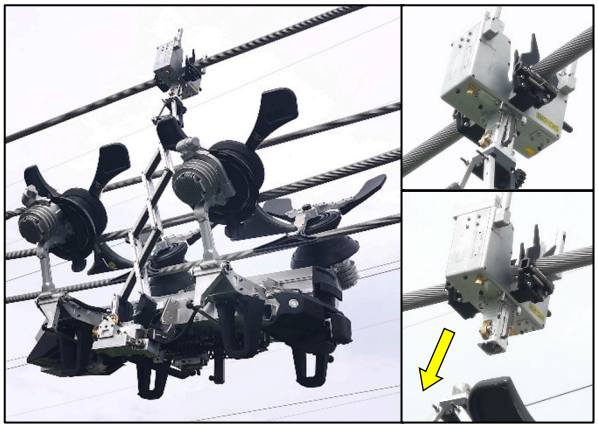

Figure 11. Lashing mechanism and sensor deployed with LineRanger.

IV. Self-Centering 360° Scanning Device

As briefly discussed in Section III, the thermal modelling of current bearing conductors incorporates the effect of sun radiations. Average surface properties (solar absorptivity and infrared emissivity) are usually used, but surface finish of live conductor may see deterioration over long periods of time due to environmental effects: pollution, highways, industries, acid rain, etc. To assess the surface finish properties and identify how these evolve with time, a novel sensor, tagged *Helios* was designed along with an optical apparatus and ground calibration method [18].

For this sensor to accurately perform *in*-situ measures, the optical system needs to complete circumferential scans of the conductor, while being guided by an open-shape motorized mechanism. Furthermore, it needs to be precisely self-centered on conductors that vary from 20 to 36 mm in diameter. Finally, the sensor is light sensitive so the mechanism must block as much sunlight as possible.

A. *Design of an open shape cylinder rotating mechanism*

The mechanism with the sensor is intended to be deployed with a robotic arm on LineRanger. Hence, the shape must be partially opened while allowing complete rotation. A double C-shape rotor/stator mechanism with the sensor installed inside the rotor that rotates on small bearings mounted on the

stator fulfils the task (Figure 12, top). The opening allows the insertion of the larger conductor (~40 mm), and the rotor diameter is large enough to be firmly located inside de stator during rotation even with partial support over the openings.

Continuous motion is ensured by a double pinion gear systems allowing the rotor to be driven during a complete rotation. Both pinions are synchronized with timing belts and pulleys: a pinion takes the relay of the other when necessary.

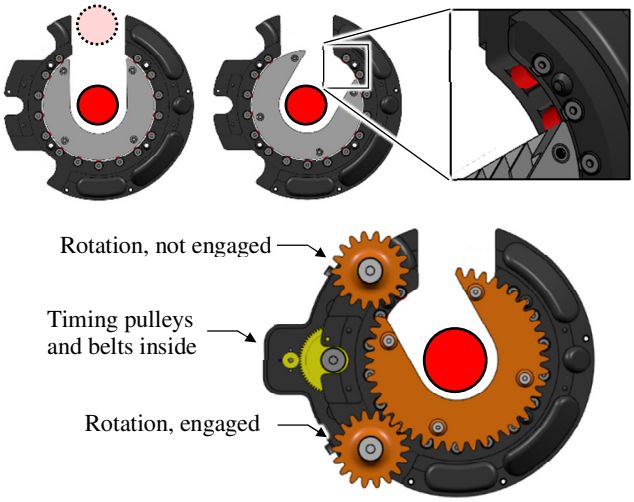

Figure 12. Open-shape cylinder rotating mechanism.

B. *Design of self-centering self-locking mechanism*

The probe deployment involves an approach phase in the direction of its opening, like both previous probes. Then, to be coaxial to the rotor, the conductor must be accurately positioned in the approach direction and in the direction perpendicular to it without touching the rotor. For ease of deployment by a teleoperated robot, centering must be done by the insertion of the conductor itself rather than by an actuator. Once inserted in the probe, the conductor must be naturally held in place, requiring the mechanism to be self-locking. Existing mechanisms are either closed (lens mount), need an actuator (tubing holder) or are partially self-locking.

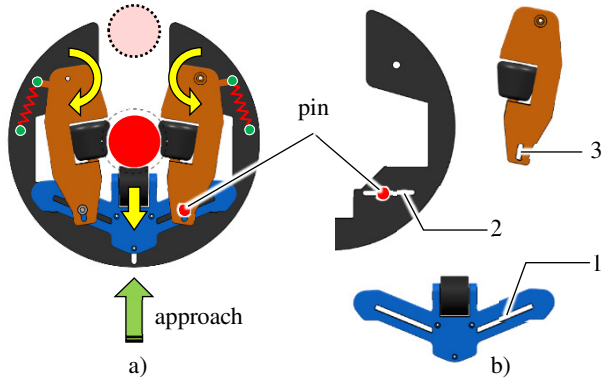

Figure 13. Self-centering concept.

The chosen design consists of rotating spring-loaded orange arms that are pushed apart at the same time by the conductor itself while inserted (Figure 13a). Their spacing then force a bottom blue part to slide down and automatically adjusts its depth depending on the diameter of the conductor. Orange and blue parts are linked together by the mean of free pin sliding in specific grooves (red dot on the figure). Groove 1 deals with self-locking and with the major portion of vertical travel of the blue part. Groove 2 finely synchronizes vertical travel of blue part with the rotation of the orange part. This groove could be linear (Figure 13b), circular or other shape. Groove 3 allows the pin to freely move relative to orange part.

To be viable, this design must overcome three challenges. 1/ The whole movement of the parts must keep the conductor coaxial to the rotor whatever its diameter. 2/ Once at the bottom, the applied force must not create a movement of the orange arms i.e., the arms drive the blue sliding part, but this one must not back-drive the orange arms. 3/ A change of lateral force that pushes on either one of orange arms must not make either arm to move, nor the bottom part, so that coaxiality is assured. Arms' spring-loading is also required.

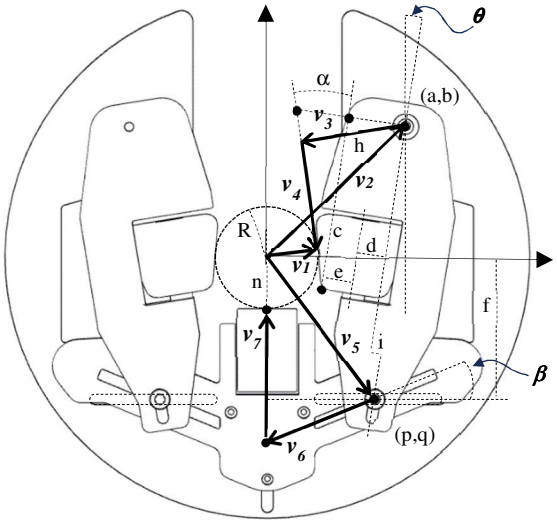

Figure 14. Self-centering design parameters.

To have a non-back-drivable mechanical system, the friction force analysis between the sliding blue plastic part and a steel pin or radius r is performed. For self-locking properties with surfaces of $\mu = 0.2$, the angle β of the groove 1 (Figure 14) must be below 22.6° after solving equation (8).

$$-rsin\beta cos\beta + \mu cos\beta(r + rcos\beta) = 0 \quad (7)$$

$$-sin\beta + \mu cos\beta + \mu = 0 \quad (8)$$

Hence, any additional force from the deploying arm on the blue part will not generate rotation of any orange arms. Similarly, a lateral force on either arm would push down the blue part that would be held by the friction with the opposite arm. This constraint on β then leads to a parametrization and optimization of the mechanism to assess the coaxiality requirement.

Initial values must first be determined. Figure 15 shows a simulation without centering mechanism as well as two non optimized mechanisms for which the dimensions are intuitively set to be compact. The first one is for a mechanism with the pins fixed on the arms and the second one, with a free pin moving in the linear groove 2 considered above. A linear groove is chosen for the geometrical optimization because its curve is flatter. Hence, knowing that:

$$\boldsymbol{v_1 = v_2 + v_3 + v_4} \quad (9)$$

$$\boldsymbol{v_1} = \boldsymbol{v_2} - \frac{\|v_2\|}{\|v_1\|}\boldsymbol{v_1} + \frac{\|v_4\|}{\|v_1\|}\begin{bmatrix} 0 & 1 \\ -1 & 0 \end{bmatrix}\boldsymbol{v_1} \quad (10)$$

$$r\begin{bmatrix} cos(\gamma) \\ sin(\gamma) \end{bmatrix} = \begin{bmatrix} a \\ b \end{bmatrix} - h\begin{bmatrix} cos(\gamma) \\ sin(\gamma) \end{bmatrix} + \|\boldsymbol{v_4}\|\begin{bmatrix} sin(\gamma) \\ -cos(\gamma) \end{bmatrix} \quad (11)$$

Defining $g = d + e + c\tan\alpha$, $h = g\cos\alpha$ and $\gamma = \alpha - \theta$, using the "x" terms of equation (11) to find $\|\boldsymbol{v_4}\|$, then inserting in the "y" terms and use (12) to find q with (13):

$$sin\,\theta = \frac{2t}{1+t^2} \quad \text{and} \quad cos\,\theta = \frac{1-t^2}{1+t^2} \quad (12)$$

$$t = \frac{2b \pm \sqrt{4b^2 - 4(R+h+a)(R+h-a)}}{2(R+h+a)} \quad (13)$$

Then, for the sliding blue part,

$$\boldsymbol{v_8} = \boldsymbol{v_5} + \boldsymbol{v_6} + \boldsymbol{v_7} \quad (14)$$

$$\begin{bmatrix} 0 \\ n \end{bmatrix} = \begin{bmatrix} p \\ -f \end{bmatrix} - \frac{p}{cos\beta}\begin{bmatrix} 1 \\ sin\beta \end{bmatrix} + \begin{bmatrix} 0 \\ j \end{bmatrix} \quad (15)$$

$$p = a - (b + f)\,tan\,\theta + \frac{i}{cos\,\theta} \quad (16)$$

And finally, the vertical misalignment *MIS* between the desired position of the conductor's axis and the position given by the mechanism can be found with:

$$MIS = -f - (tan\,\beta)\,p + j - n + R \quad (17)$$

This equation is based on all the geometrical parameters of the mechanism which can be optimized with *Matlab* to eventually minimize (17) for any diameter of the conductor. Considering the geometric limitation during the optimization, the parameters ranges are restricted within specific values.

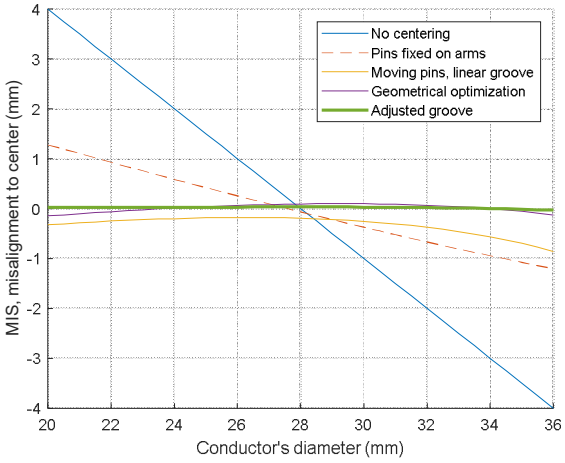

Figure 15. Self-centering study and optimization.

The geometrical optimization largely improves the curve's flatness and has a max error in the range of machining processes. For any conductor diameter, the axial centering is nearly perfect from a practical point of view. However, a final adjustment is possible with a *nearly* linear groove to get a perfect centering while keeping self-locking property.

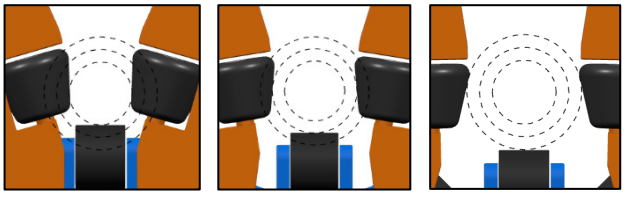

Figure 16. Self-centering validation.

The mechanism is then modelized with its final dimensions and the centering is verified with CAD simulations (Figure 16). That being confirmed, all previous sub-mechanisms are then merged to get a complete operational self-centering 360° rotational device (Figure 17). The optical sensor in internally mounted in the rotor but its design and analysis are beyond the scope of this paper.

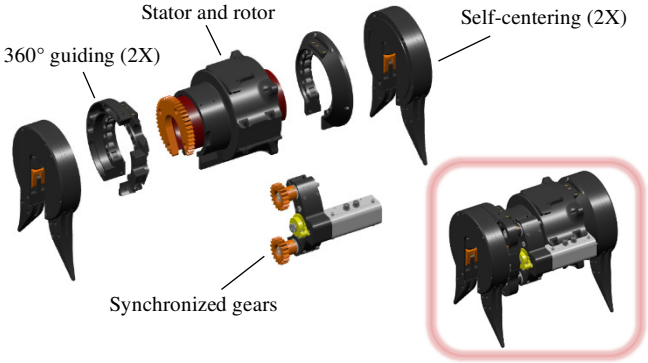

Figure 17. Self-centering 360° device model.

C. *Field deployment*

Field trials of this new application were recently performed on several 735 kV spans, confirming previous insights about non-uniformity of conductor's surface properties around its circumference. The *Helios* mechanism performed well, providing enough rigidity for the optical system. Also, because the scanned lined were made of different conductors, the auto-centering function proved efficient and essential, since the exact diameter of a given span is sometime unknown. This mechanical design opens the way for other types of application: cleaning, paint application, repair, etc.

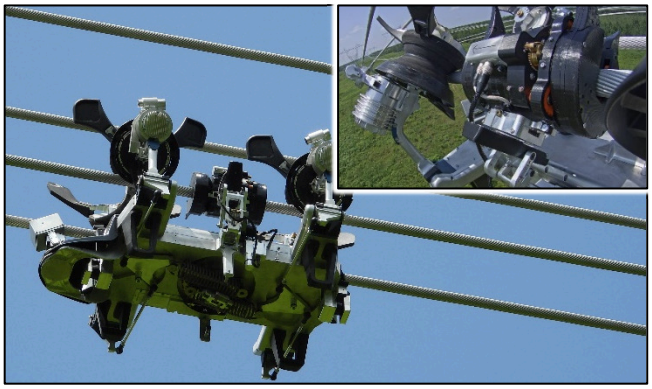

Figure 18. Self-centering 360° device model.

V. Conclusion

In this paper, three (3) novel mechanisms were designed to minimize the control electronics and number of actuators, along with LineRanger's design philosophy. Recent successful field deployments of these applications were found relevant for asset management personal, as they broaden the scope of work of this robotic solution. It is believed that these new applications, the design philosophy, and their successful field utilization could inspire and stimulate the robotics community to further tackle challenges associated with powerline inspection and maintenance.

REFERENCES

[1] F. Mirallès et al., "LineDrone Technology: Landing an Unmanned Aerial Vehicle on a Power Line," 2018 IEEE International Conference on Robotics and Automation (ICRA), Brisbane, QLD, Australia, 2018, pp. 6545-6552, doi: 10.1109/ICRA.2018.8461250.

[2] P. Hamelin *et al*., "Discrete-time control of LineDrone: An assisted tracking and landing UAV for live power line inspection and maintenance," *2019 International Conference on Unmanned Aircraft Systems (ICUAS)*, Atlanta, GA, USA, 2019, pp. 292-298, doi: 10.1109/ICUAS.2019.8798137.

[3] Pouliot, N., Lavoie, E., Rousseau, G., & Montambault, S. (2014, October). An integrated approach for non-destructive testing of ACSR conductors: Early deployments of robotized sensors. In Proceedings of the 2014 3rd International Conference on Applied Robotics for the Power Industry (pp. 1-6). IEEE.

[4] Pouliot, N., Lavoie, E., Rousseau, G., Leblond, A., Brissette, A., & Montambault, S. (2015, October). Non-Destructive Evaluation Technologies for Assessing Large River Crossing Conductors, Prior to Restringing. In 2015 CIGRÉ Conference on Condition Monitoring, Diagnosis and Maintenance.

[5] Pouliot, N., & Montambaut, S. (2017, April). Sensors for the non-destructive evaluation of ACSR, deployed with live-line robotics. In 2017 12th International Conference on Live Maintenance (ICOLIM) Strasbourg, 2017.

[6] Bellemare, J., Rousseau, G. A., Valiquette, D., Sirois, F., & Pouliot, N. (2021). Reporting on the last 6 years of field inspections using LineCore for the non-destructive evaluation of overhead conductors.

[7] F. Wang et al., "Internal Defect Detection of Overhead Aluminum Conductor Composite Core Transmission Lines With an Inspection Robot and Computer Vision," in IEEE Transactions on Instrumentation and Measurement, vol. 72, pp. 1-16, 2023, Art no. 3512516, doi: 10.1109/TIM.2023.3265104.

[8] Ahmad Bala Alhassan, Xiaodong Zhang, Haiming Shen, Haibo Xu, Power transmission line inspection robots: A review, trends and challenges for future research, International Journal of Electrical Power & Energy Systems, Volume 118, 2020, 105862, ISSN 0142-0615.

[9] M. Chen, Y. Cao, Y. Tian, E. Li, Z. Liang and M. Tan, "A Passive Compliance Obstacle-Crossing Robot for Power Line Inspection and Maintenance," in *IEEE Robotics and Automation Letters*, vol. 8, no. 5, pp. 2772-2779, May 2023, doi: 10.1109/LRA.2023.3261704.

[10] GAO, Yuan, SONG, Guangming, LI, Songtao, et al. LineSpyX: A power line inspection robot based on digital radiography. IEEE Robotics and Automation Letters, 2020, vol. 5, no 3, p. 4759-4765.

[11] Li X, Shang D, Li F, Chen R. The climbing performance analysis of a robot for power line inspection with retractable double serial manipulators. Proceedings of the Institution of Mechanical Engineers, Part C: Journal of Mechanical Engineering Science. 2022;236(9):4946-4961. doi:10.1177/09544062211054984

[12] X. Yue, Y. Liu, H. Wang and Y. Feng, "Development of a power line Inspection Robot Capable of automatically crossing Obstacles," 2022 5th World Conference on Mechanical Engineering and Intelligent Manufacturing (WCMEIM), Ma'anshan, China, 2022, pp. 795-799, doi: 10.1109/WCMEIM56910.2022.10021526.

[13] Mendoza, N., Nemati, H., Haghshenas-Jaryani, M., & Dehghan-Niri, E. (2022, October). An Inflatable Soft Crawling Robot With Nondestructive Testing Capability for Overhead Power Line Inspection. In ASME International Mechanical Engineering Congress and Exposition (Vol. 86670, p. V005T07A021). American Society of Mechanical Engineers.

[14] Richard, P. et al. "LineRanger: Analysis and Field Testing of an Innovative Robot for Efficient Assessment of Bundled High-Voltage Powerlines." 2019 International Conference on Robotics and Automation (ICRA), 2019: 9130-9136.

[15] YouTube. (2018). LineRanger: A Revolution in Transmission Line Robotics. [online] Available at: https://www.youtube.com/watch?v=OItActG9S6U

[16] P. Hamelin et al., "Slip-Limiting Controller for Redundant Line-Suspended Robots: Application to Line Ranger," 2020 IEEE International Conference on Robotics and Automation (ICRA), 2020, pp. 7081-7087, doi: 10.1109/ICRA40945.2020.9196832.

[17] P. -L. Richard *et al*., "Inside LineRanger: Mechanism Design to Optimize Operation and Performances of Powerline Inspection Robot," *2022 International Conference on Robotics and Automation (ICRA)*, Philadelphia, PA, USA, 2022, pp. 8157-8163, doi: 10.1109/ICRA46639.2022.9811366.

[18] Bellemare, J. *et al.,* "In-situ evaluation of ACSR Absorptivity Using Helios, a Novel Probe Deployed by Robotic Means". Submitted for publication to the 2024 CIGRÉ General Meeting, Paris, August 2024